ARTICLE

https://doi.org/10.1590/2317-4889202020190085

BJGEO Brazilian Journal of Geology

Parauapebas meteorite from Pará, Brazil, a "hammer" breccia chondrite

Daniel Atencio[1]*, Dorília Cunha[1], André Luiz Ribeiro Moutinho[2], Maria Elizabeth Zucolotto[3], Amanda Araujo Tosi[3], Caio Vidaurre Nassif Villaça[3]

Abstract

The Parauapebas meteorite, third official meteorite discovered in the Brazilian Amazon region, is a "hammer meteorite" which fell on December 9th, 2013, in the city of Parauapebas, Pará State, Brazil. Mineralogy is dominated by forsterite, enstatite, iron, troilite, and tetrataenite. Albite, chromite, diopside, augite, pigeonite, taenite, and merrillite are minor components. Two main clasts are separated by black shock-induced melt veins. One clast exhibits an abundance of chondrules with well-defined margins set on a recrystallized matrix composed mostly of forsterite and enstatite, consistent with petrologic type 4 chondrites. The other clast displays chondrules with outlines blurring into the groundmass as evidence of increasing recrystallization, consistent with petrologic type 5 chondrites. The clasts of petrologic type 4 have a fine-grained texture compared to those of type 5. It is a genomict breccia (indicated by shock melt veins) with the clasts and matrix of the same compositional group, but different petrologic types, H4 and H5. The melted outer crust of the Parauapebas meteorite is comprised of forsterite with interstitial dendritic iron oxide, and is rich in irregular vesicles, which are evidence of the rapid formation of the crust. The type specimen is deposited in the Museum of Geosciences of the University of São Paulo, Brazil.

KEYWORDS: Parauapebas; meteorite; chondrite; breccia; Brazilian meteorite.

INTRODUCTION

Parauapebas is the third official meteorite found in the state of Pará, along with the Ipitinga chondrite, H5, found in the Ipitinga mountain range, Almeirim city, in 1989 (Dreher *et al.* 1995), and Serra Pelada, a rare anomalous brecciated eucrite that fell in the famous village of Serra Pelada, city of Curionópolis, in 2017 (Zucolotto *et al.* 2018, Yin *et al.* 2019). Parauapebas is also the first recognized meteorite fall of Pará State, despite the fact that Serra Pelada meteorite was classified and made official first. This happened because the meteorite was kept with the finders for about 5 years before it was made available to researchers for classification.

Parauapebas is a "hammer" meteorite, a term associated with meteorites that strike objects or people during their fall. There is one very well-documented case of a meteorite that struck and injured a person, the Sylacauga meteorite (Swindel Jr. and Jones 1954), which fell in 1954 in Alabama, USA, hitting and wounding Mrs. Ann Hodges. In the case of Parauapebas, the event took place about 5 years ago and it was not possible to obtain evidence such as photos of Mrs. Maria das Neves's injury (see below). However, both Maria das Neves's and her son's testimonials were obtained and recorded, reporting the occurrence of the injury.

For the classification and officialization of this meteorite by the Nomenclature Committee of the Meteoritical Society, a consortium was established between researchers of the Institute of Geoscience of the Universidade de São Paulo and the Brazilian National Museum, Universidade Federal do Rio de Janeiro.

During the submission of the Parauapebas meteorite, the Museum of Geoscience of the Universidade de São Paulo was registered in the Nomenclature Committee of the Meteoritical Society as an official repository of meteorite type specimens. The Parauapebas meteorite is the first meteorite whose type sample is deposited in this museum. The type specimen deposited in the Museum of Geosciences (34.8 g) belongs to the fragment that caused injuries to Mrs. Maria das Neves. Another 4g of the same fragment was deposited in the National Museum of Rio de Janeiro. Andre L. R. Moutinho holds the 210.3 g main mass and a 13.08 g slice of the Mrs. Maria das Neves fragment.

Fall circumstances

On December 9th, 2013, about 7:00 p.m. local time, a meteorite fell in the city of Parauapebas (6°2'55.7"S 49°53'19.3"W), located in the eastern part of Pará State, Brazil (Fig. 1).

[1]Universidade de São Paulo – São Paulo (SP), Brazil.
E-mails: datencio@usp.br, doriliacunha@gmail.com

[2]International Meteorite Collector Association – Jacareí (SP), Brazil.
E-mail: moutinho@gmail.com

[3]Universidade Federal do Rio de Janeiro – Rio de Janeiro (RJ), Brazil.
E-mail: meteoritos@mn.ufrj.br, amandatosi@hotmail.com, caiovillaca@yahoo.com.br

*Corresponding author.

A witness reported seeing the bolide traveling from NE to SW direction. A stone hit the roof of a house with a loud noise that was heard by resident Mrs. Maria das Neves Silva Lima. She claims that a meteorite fragment hit and injured her right shoulder, but her son says that she was hit only by roof debris. Her son, Ilson Silva Lima, collected the stone on the roof. The stone broke into two pieces during the impact. One piece is lost, but the remaining fragment of 62 grams (Fig. 2) was kept by Mrs. Maria das Neves until 2015, when she handed it over to Dorília Cunha, who was working at the USP's Institute of Geosciences at the time. Mrs. Maria das Neves is the mother of Dorilia's sister-in-law. She took the meteorite to be studied by some people who did not show much interest. Finally, she managed to attract the attention of Professor Daniel Atencio and, together, they began the first analyses. The Parauapebas meteorite was finally approved on December 2nd, 2018.

Another stone from this same fall, showing flight orientation features and weighing 210.3 g (Fig. 3), was also witnessed to fall by other residents of the city while they were in front of their houses. Meire C. Rosa, her husband Paulo T. Nunes, her mother Rosa C. Santos, and their neighbors heard a loud noise of thunder and the impact when the stone struck the wooden beam of the roof of their house and then fell, embedding itself on the ground. Meire immediately picked up the stone and noticed that it was still warm. In early 2018, she contacted André L.R. Moutinho, who was already part of the classification team of the 62 g fragment. The 210.3 g stone was purchased by André L. R. Moutinho.

METHODS

Slices were examined using a stereomicroscope Zeiss Discovery V8. Polished thin sections were examined microscopically in transmitted and reflected light using a Zeiss Axioplan petrographic microscope.

Quantitative analyses of the constituent phases were carried out using the JEOL EPMA JXA-8230 Superprobe at LABSONDA/IGEO/UFRJ, WDS mode. Beam conditions included an accelerating voltage of 15 keV for silicates and 20 keV for opaque minerals, beam current of 20nA, and a spot size of 1 μm. Natural and synthetic standards of well-known compositions were used as standards for wavelength dispersive spectrometry (Tab. 1).

Corrections for differential matrix effects were made with a ZAF factory-supplied procedure. In total, 45 olivine and 32 pyroxene grains were analyzed. Points in the cores and rims of the grains were analyzed in order to access their compositional ranges. Energy Dispersive Spectrometer (EDS) data were also obtained at the Institute of Geoscience, Universidade de São Paulo.

The cathodoluminescence (CL) color image was obtained by the electron beam source CITL MK5-2, attached to the petrographic microscope Zeiss Axio Imager 2 under such analytical condition: the voltage applied was 15 keV and the current was 0.7 mA in a vacuum condition. In this way, a cooled charge-coupled device (CCD) camera recorded the real color emitted by the minerals as a luminescence response. From the CL images obtained from each piece of the meteorite, it was possible to create a photomosaic through the Adobe-Bridge CS6-64bit and the final

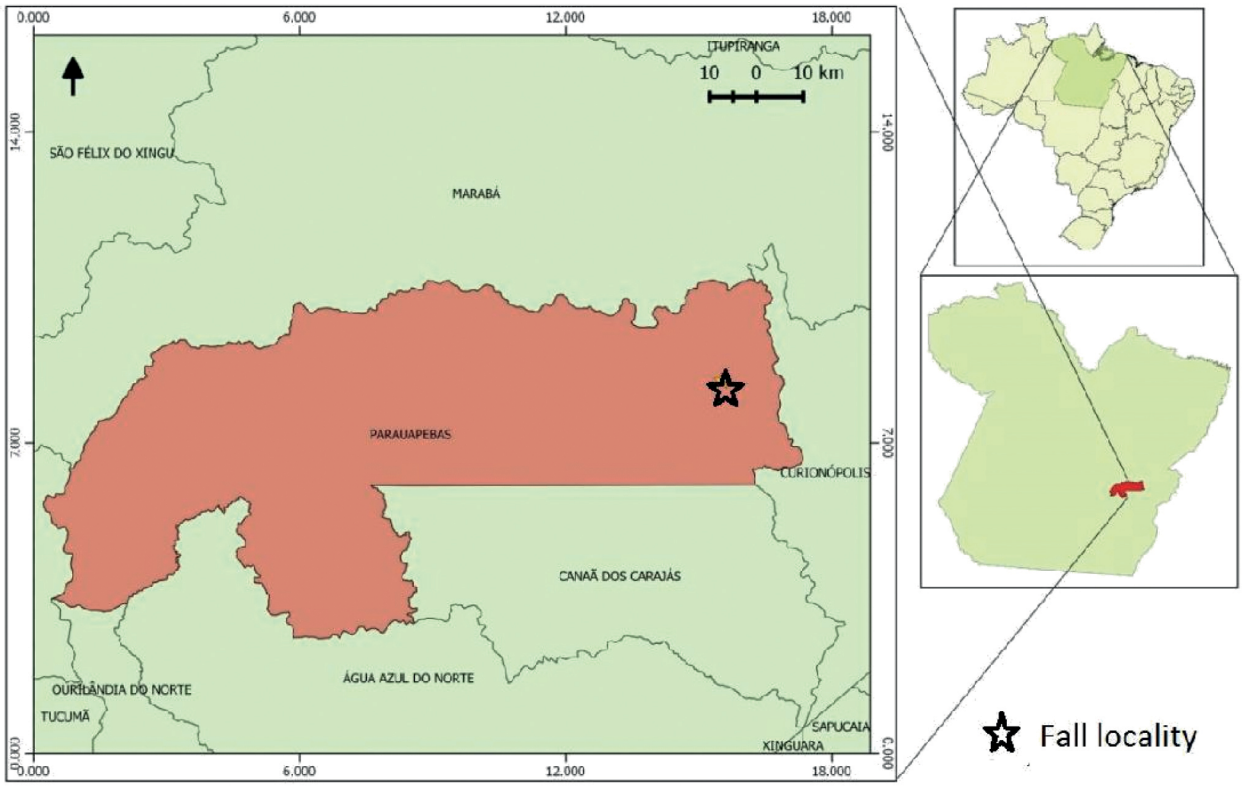

Figure 1. Parauapebas meteorite fall location.

treatment of the image was done in the Adobe-Photoshop CS6-64bit software.

Physical characteristics

The 210.3 g main mass is almost fully crusted. It measures 5.7 × 5.3 × 4.2 cm, and shows orientation features such as nose-cone shape and roll-over lips. A small portion of the secondary crust is also present. The 62 g fragment measures 4.8 × 3.5 × 2.6 cm.

Fusion crust is dull black with 0.1 to 0.2mm in thickness in the entire observed sample. A variation in thickness may be present on the different masses as a result of

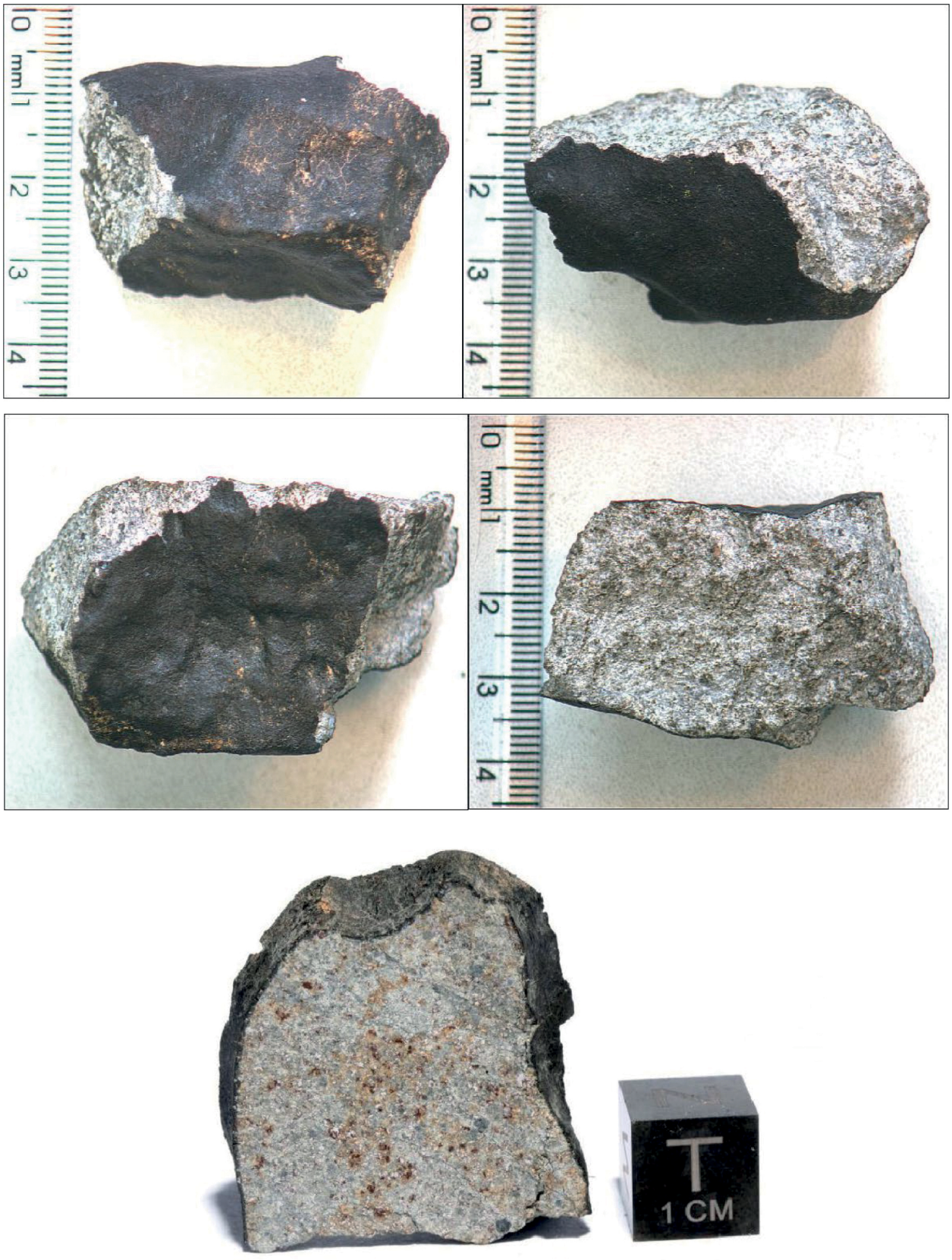

Figure 2. Parauapebas meteorite 62 g fragment.

in-flight fragmentation. On one side, it shows markedly regmaglypts. The fresh fractures surfaces of the meteorite interior have a variable gray color with a rare indication of brecciation.

Figure 3. Parauapebas meteorite 210.3 g oriented main mass. Note the nose-cone and roll over lips features.

Table 1. Standards used for microprobe analyses.

Olivine and Pyroxene	
Al, Si, Mg, Fe, Ca, Cr, Mn	Cr-bearing augite – Smithsonian
Ti	Kakanui hornblende – Smithsonian
Mn	Bustamite – Astimex
Plagioclase	
Na, Al, Ca	Plagioclase An65 – Astimex
Si, K	Anortite – Smithsonian
Mg, Fe, Mn	Augite – Smithsonian
Cr	Cr-bearing augite – Smithsonian
Ti	Basaltic glass – Smithsonian
Opaque minerals	
Fe	Pyrite – Astimex
Ni	Ni – Astimex
S	Pyrite – Astimex
P	Apatite – Astimex
Al	Al – Astimex
Cr	Cr – Astimex
Ti	Apatite – Astimex
Co	Co – Astimex
Si	Quartz – Astimex

Very thin black veinlets can be discerned in the interior of some broken and cut surfaces and resemble shock veins. On some cut surfaces, the slice fast becomes stained due to the high iron content.

Texture

In the examined thin section, the meteorite shows a well-developed chondritic texture, being possible to observe two main clasts separated by some black shock-induced melt vein crossing the entire thin section (Fig. 4). One clast (above the melt vein) exhibits an abundance of chondrules with well-defined margins, ranging in size from 0.3 to 0.9 mm, set on a microcristalline partial recrystallized matrix composed mostly by olivine and pyroxene, consistent with petrologic type 4 chondrites. The other clast displays less discernible chondrules of the same apparent dimensions, but with the outlines blurring into the groundmass, as evidence of increasing recrystallization, consistent with petrologic type 5 chondrites. Both clasts exhibit chondrules with variable internal texture such as porphyritic chondrules: PO (porphyritic olivine), PP (porphyritic pyroxene), POP (porphyritic olivine and pyroxene); non-porphyritic chondrules: GOP (granular olivine and pyroxene), C (cryptocrystalline), RP (radiating pyroxene), BO (barred olivine); and many chondrule fragments. The clasts of petrologic type 4 have a fine-grained texture compared to those of type 5. It is a genomict breccia (indicated by shock melt veins) with the clasts and matrix of the same compositional group but different petrologic types, H4 and H5.

Mineralogy and chemical composition

Mineralogy is dominated by forsterite, enstatite, iron, troilite, and tetrataenite. Albite, chromite, diopside, augite, pigeonite, taenite, and merrillite are minor components (Fig. 5). Microprobe analyses of each mineral both in the chondrules and in the matrix, in type 4, type 5 and the veins were treated separately, in an attempt to verify whether there were compositional differences among the lithologies. However, a rather homogeneous chemistry was found in the whole section, even presenting discernible textures.

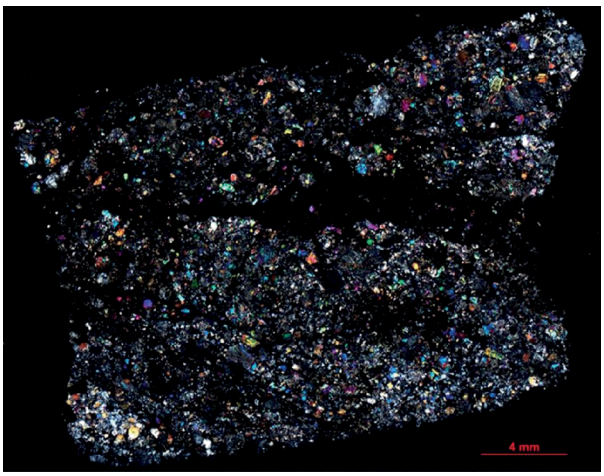

Figure 4. Parauapebas meteorite thin section under cross-polarized light (XPL) showing the two main clasts separated by a vein.

Forsterite, $Mg_2(SiO_4)$

Most forsterite crystals show undulatory extinction and irregular fractures, and few have weak mosaicism. Chemical data for forsterite are represented in Figure 6 and in Table 2. The observed Fa indices are characteristic of H chondrites.

Pyroxene group minerals

Enstatite, $Mg_2Si_2O_6$, pigeonite, $(Mg,Fe,Ca)_2Si_2O_6$, augite, $(Ca,Mg,Fe)_2Si_2O_6$, and diopside, $CaMgSi_2O_6$ (Tab. 3) were chemically identified. Values of Fs-En-Wo are included in the cited table. Ternary diagram showing type 4, 5 and veins pyroxene analyses are represented in Figure 6. Most Fs indices for enstatite are characteristic for H chondrite, except for a few typical points of L-chondrites.

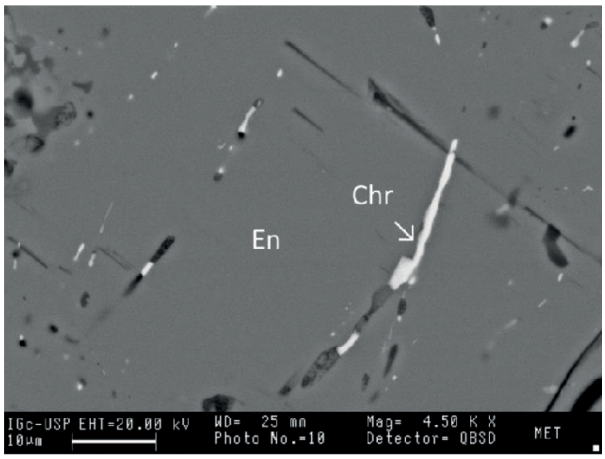

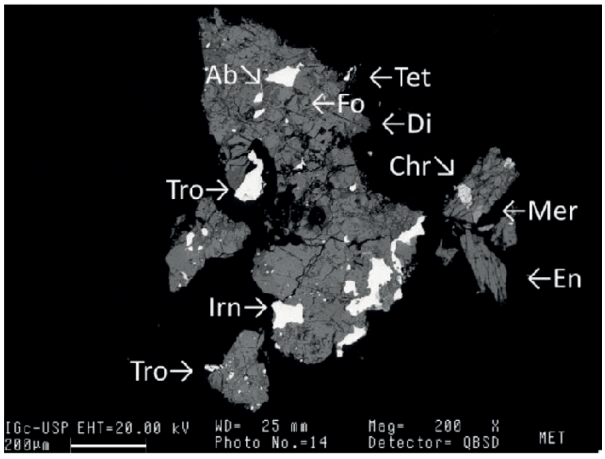

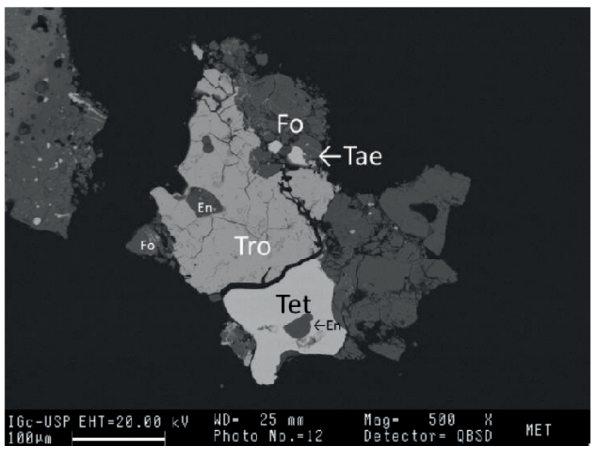

Ab: albite; Chr: chromite; Di: diopside; En: enstatite; Fo: forsterite; Mer: merrillite; Tae: taenite; Tet: tetrataenite; Tro: troilite.

Figure 5. Backscattered images.

Albite, $Na(AlSi_3O_8)$

Albite forms small secondary crystals. Chemical data and Ab-An-Or values are in Table 4 and Figure 6.

Iron, Fe; Tetrataenite, FeNi; Taenite, (Fe,Ni); and Troilite, FeS

Iron analyzed under reflected light shows Neumann bands, which are mechanical twins on the {211} planes. Twinning is induced by shock, either due to collisions in space, or during atmospheric passage. The ubiquity of Neumann bands indicates that they are easily formed at relatively low levels of shock (Buchwald 1975). In the past, the name "kamacite" was applied to iron from meteorite, but this unnecessary name was discredited by Burke (2006). Intimate intergrowth of iron and taenite ("plessite texture") with associated tetrataenite was observed. Zoned taenite could also be seen.

Chemical data and the calculated empirical formulas for iron, tetrataenite, and taenite are reported in Table 5. Troilite chemical data and the calculated empirical formulas are in Table 6.

Chromite, $Fe^{2+}Cr_2O_4$; and Merrillite, $Ca_9NaMg(PO_4)_7$

Chromite and merrillite are rare in the Parauapebas meteorite and only were identified by scanning electron microscopy/energy dispersive X-Ray spectroscopy (SEM/EDS) in broken fragments produced during the making of slides. There is no reference about where (H4, H5, vein, chondrule/matrix) chromite and merrillite were analyzed. Chromite occurs as platelet-shaped inclusions, which is relatively common in meteorites, or as irregular grains (Fig. 5). Only one set of EDS chemical data for each habit type were obtained and they are very similar. Mean values are: FeO 28.65, MgO 2.74, MnO 1.04, CaO 0.50, Cr_2O_3 54.80, Al_2O_3 6.33, SiO_2 1.06, TiO_2 1.63, V_2O_5 0.76, total 97.51 wt%. The calculated empirical formula is $(Fe^{2+}_{0.86}Mg_{0.15}Mn^{2+}_{0.03}Ca_{0.02})_{\Sigma1.06}(Cr_{1.55}Al_{0.27}Si_{0.04}Ti_{0.04}V^{5+}_{0.02})_{\Sigma1.92}O_4$.

Only one merrillite grain was verified (Fig. 5). EDS data (one point analyzed) are CaO 45.12, Na_2O 2.46, MgO 3.59, FeO 0.76, P_2O_5 48.46, SiO_2 0.82, total 101.21 wt%. The calculated empirical formula is $Ca_{8.41}Na_{0.83}(Mg_{0.93}Fe^{2+}_{0.11})_{\Sigma1.04}Si_{0.14}P_{7.14}O_{28}$.

Fusion crust

The melted outer crust of the Parauapebas meteorite (Fig. 7) is comprised of forsterite with interstitial dendritic iron oxide. We cannot confirm if this iron oxide is magnetite, wüstite or other species because the dendrites are too small for accurate quantitative analyses. Qualitative EDS analyses indicate the occurrence of not only Fe but also of Mg, Si, and other elements due to matrix overlap with the forsterite surrounding phase. The molten crusts of meteorites are usually metal free, that is, the dendrites are probably not composed by metallic iron. The melted crust

of the Parauapebas meteorite is rich in irregular vesicles. The presence of vesicles and iron oxide dendrites are evidence of the rapid formation of the crust. Detailed studies of meteorite fusion crusts were made by Ramdohr (1967) and Hezel *et al.* (2015).

DISCUSSION

According to the textural scheme of Gooding and Keil (1981), recognizable chondrule texture are: BO, PO chondrules, and RP crystals. Olivine crystals with undulatory extinction and irregular fractures, and a weak mosaicism,

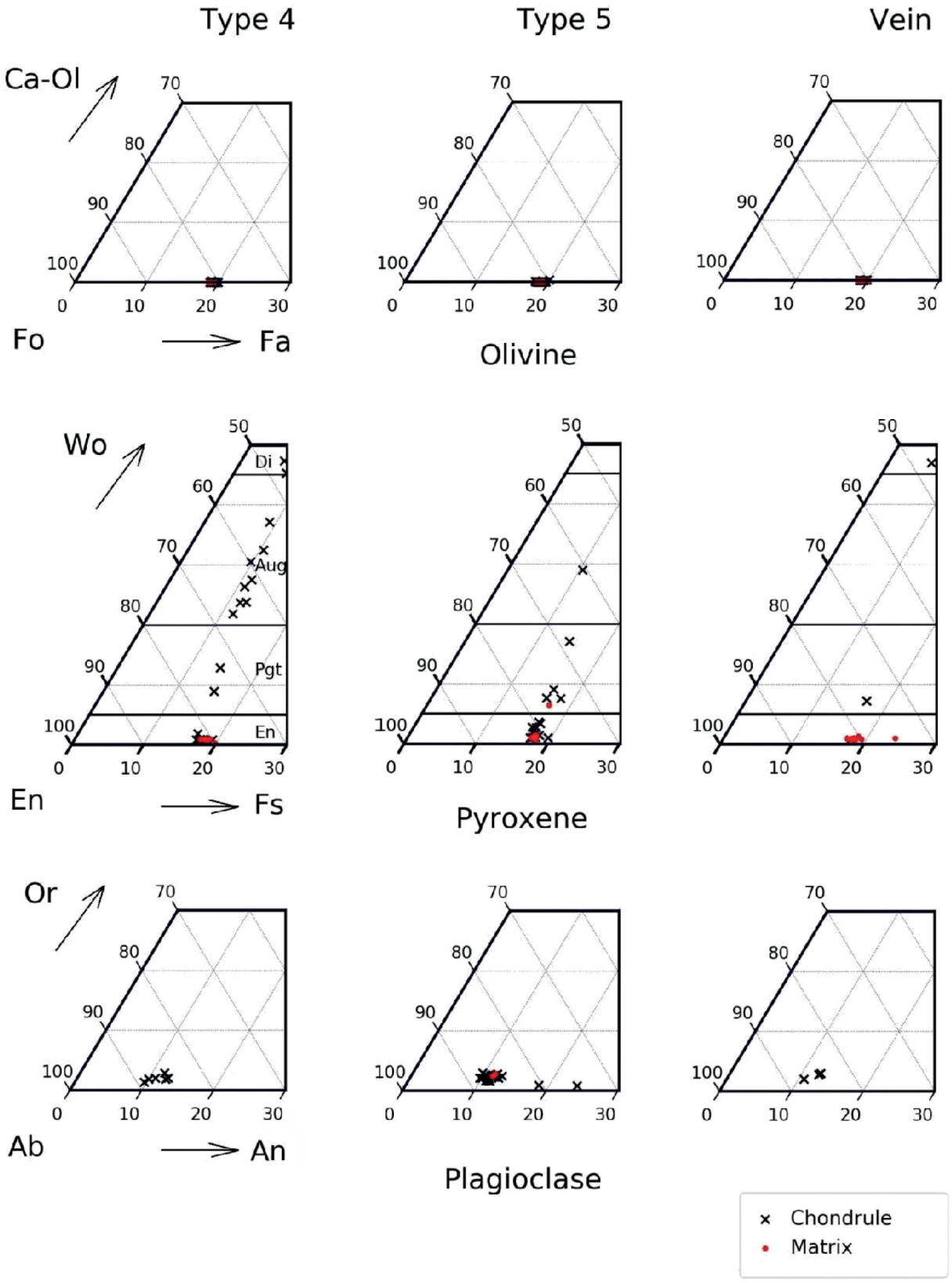

Ab: albite; An: anorthite; Aug: augite; Ca-ol: calcio-olivine; Di: diopside; En: enstatite; Fa: fayalite; Fo: forsterite; Fs: ferrosilite; Or: orthoclase; Pgt: pigeonite; Wo: wollastonite.

Figure 6. Olivine, pyroxene, and plagioclase ternary diagrams.

Table 2. Microprobe data for forsterite (wt.%).

	Type 4 – chondrule	Type 4 – matrix	Type 5 – chondrule	Type 5 – matrix	Vein – chondrule	Vein – matrix
n	**12**	**3**	**39**	**6**	**8**	**7**
CaO	0.03 (0.00–0.21)	0.00 (0.00–0.00)	0.02 (0.00–0.23)	0.01 (0.00–0.03)	0.04 (0.00–0.11)	0.01 (0.00–0.02)
MgO	41.36 (40.43–42.16)	41.31 (40.28–42.19)	41.81 (39.13–42.88)	41.78 (40.89–42.70)	41.27 (40.59–42.07)	41.72 (40.47–42.69)
FeO	17.68 (17.22–18.27)	17.37 (16.87–17.67)	17.41 (16.58–18.04)	17.44 (17.07–17.79)	17.68 (16.92–18.28)	17.79 (17.40–18.58)
MnO	0.48 (0.44–0.53)	0.51 (0.49–0.53)	0.46 (0.41–0.49)	0.47 (0.44–0.50)	0.46 (0.43–0.51)	0.46 (0.43–0.50)
Al_2O_3	0.02 (0.00–0.08)	0.01 (0.00–0.01)	0.06 (0.00–1.57)	0.01 (0.00–0.03)	0.08 (0.01–0.39)	0.02 (0.00–0.11)
Cr_2O_3	0.05 (0.01–0.41)	0.02 (0.00–0.04)	0.09 (0.00–1.51)	0.01 (0.00–0.03)	0.04 (0.00–0.11)	0.01 (0.00–0.03)
SiO_2	39.35 (38.52–40.56)	39.79 (38.91–41.46)	39.33 (37.62–40.96)	38.97 (38.29–39.97)	39.54 (39.19–40.34)	39.28 (38.32–39.75)
TiO_2	0.05 (0.00–0.20)	0.03 (0.01–0.04)	0.02 (0.00–0.11)	0.01 (0.00–0.02)	0.01 (0.00–0.07)	0.02 (0.00–0.07)
Total	99.02 (98.01–99.87)	99.04 (97.78–99.87)	99.20 (97.50–100.78)	98.70 (97.37–99.97)	99.12 (97.53–99.73)	99.31 (97.89–100.13)
Fa	19.23 (18.76–19.89)	18.98 (18.48–19.55)	18.84 (18.10–19.99)	18.88 (18.23–19.30)	19.27 (18.80–19.84)	19.21 (18.52–20.13)

Table 3. Microprobe data for pyroxene: enstatite (En), pigeonite (Pgt), augite (Aug), and diopside (Di) (wt.%).

	En	En	En	En	En	En
	Type 4 – chondrule	**Type 4 – matrix**	**Type 5 – chondrule**	**Type 5 – matrix**	**Vein – chondrule**	**Vein – matrix**
n	**8**	**6**	**11**	**8**	**1**	**8**
CaO	0.51 (0.34–0.97)	0.44 (0.22–0.51)	1.00 (0.54–1.79)	0.59 (0.39–0.75)	0.43	0.50 (0.40–0.70)
MgO	30.86 (29.64–33.56)	30.32 (28.98–34.24)	29.73 (27.66–30.87)	30.44 (29.71–31.73)	31.70	29.86 (28.60–30.74)
FeO	11.39 (10.47–12.86)	11.88 (10.92–14.68)	11.01 (10.02–12.75)	11.24 (10.77–11.81)	11.79	12.05 (11.01–15.84)
MnO	0.51 (0.49–0.55)	0.49 (0.47–0.51)	0.49 (0.46–0.55)	0.51 (0.48–0.52)	0.52	0.51 (0.47–0.55)
Al_2O_3	0.10 (0.05–0.22)	0.20 (0.07–0.52)	0.43 (0.08–2.19)	0.20 (0.06–0.74)	0.10	0.29 (0.11–1.12)
Cr_2O_3	0.13 (0.05–0.37)	0.14 (0.07–0.42)	0.15 (0.08–0.54)	0.10 (0.06–0.13)	0.08	0.35 (0.08–1.36)
SiO_2	55.85 (51.73–57.05)	54.83 (47.20–57.27)	56.43 (55.78–57.10)	56.10 (54.43–56.90)	55.29	55.60 (52.41–56.95)
TiO_2	0.12 (0.05–0.21)	0.13 (0.06–0.19)	0.18 (0.11–0.27)	0.14 (0.07–0.19)	0.14	0.19 (0.11–0.37)
Total	99.47 (98.60–99.78)	98.43 (97.18–99.32)	99.42 (98.63–100.45)	99.32 (98.77–100.49)	100.06	99.35 (98.41–100.27)
Fs	17.62 (16.63–19.20)	18.44 (17.42–19.81)	17.49 (16.46–19.52)	17.60 (17.20–17.96)	17.75	18.90 (17.22–23.90)
En	81.41 (79.90–82.24)	80.71 (79.82–81.60)	80.55 (79.30–81.91)	81.27 (80.84–81.77)	81.46	80.14 (75.08–81.87)
Wo	0.97 (0.65–1.88)	0.86 (0.36–1.01)	1.96 (1.01–3.69)	1.13 (0.73–1.48)	0.79	0.96 (0.75–1.35)

	Pgt	Pgt	Pgt	Pgt	Aug	Aug	Di	Di
	Type 4 – chondrule	**Type 5 – chondrule**	**Type 5 – matrix**	**Vein – matrix**	**Type 4 – chondrule**	**Type 5 – chondrule**	**Type 4 – chondrule**	**Vein – chondrule**
n	**2**	**4**	**1**	**1**	**8**	**2**	**2**	**1**
CaO	5.43 (4.35–6.50)	5.05 (3.75–7.09)	3.70	3.21	13.34 (10.09–17.31)	14.65 (14.64–14.66)	19.60 (19.42–19.79)	23.29
MgO	26.59 (26.55–26.62)	26.80 (20.44–31.90)	31.68	24.21	21.01 (18.03–24.22)	18.36 (14.71–22.00)	14.30 (13.74–14.87)	16.84
FeO	9.04 (8.83–9.24)	10.08 (7.34–11.93)	12.01	9.09	6.34 (5.12–7.72)	7.68 (6.42–8.94)	3.40 (2.93–3.86)	3.57
MnO	0.41 (0.40–0.42)	0.44 (0.38–0.48)	0.48	0.45	0.30 (0.27–0.38)	0.27 (0.23–0.31)	0.20 (0.20–0.20)	0.23
Al_2O_3	0.88 (0.37–1.39)	1.55 (0.16–4.64)	0.08	4.09	2.31 (0.27–4.81)	2.69 (0.33–5.04)	3.81 (3.24–4.37)	0.54
Cr_2O_3	0.24 (0.16–0.33)	0.22 (0.17–0.33)	0.16	0.21	0.34 (0.27–0.45)	0.43 (0.42–0.44)	0.49 (0.46–0.51)	0.77
SiO_2	55.99 (55.97–56.02)	55.07 (50.55–58.36)	51.29	57.43	54.55 (50.36–56.65)	54.28 (53.71–54.84)	55.98 (55.51–56.45)	53.53
TiO_2	0.18 (0.10–0.26)	0.19 (0.14–0.23)	0.16	0.16	0.19 (0.12– 0.27)	0.27 (0.23–0.31)	0.19 (0.18–0.19)	0.55
Total	98.76 (98.23–99.28)	99.40 (97.99–100.72)	99.56	98.85	98.38 (96.30–99.39)	98.63 (97.95–99.29)	97.97 (97.77–98.16)	99.32
Fs	14.83 (14.27–15.40)	16.19 (14.50–18.01)	16.96	16.80	10.86 (8.98–12.40)	13.67 (10.40–16.94)	6.62 (5.97–7.27)	5.98
En	74.31 (72.90–75.71)	73.47 (68.44–76.38)	76.61	75.97	61.20 (53.85–66.64)	54.50 (48.41–60.59)	47.02 (46.65–47.40)	47.15
Wo	10.86 (8.89–12.83)	10.34 (7.57–17.07)	6.43	7.24	27.92 (21.80–37.16)	31.83 (29.01–34.65)	46.30 (45.33–47.38)	46.88

Table 4. Microprobe data for albite (wt.%).

	Type 4 – chondrule	Type 5 – chondrule	Type 5 – matrix	Vein – chondrule
n	**6**	**20**	**3**	**3**
Na_2O	10.98 (10.39–11.41)	10.87 (9.44–11.55)	11.07 (10.99–11.13)	10.58 (9.63–11.30)
K_2O	0.39 (0.25–0.57)	0.42 (0.16–0.57)	0.51 (0.48–0.55)	0.49 (0.41–0.58)
CaO	2.57 (2.04–2.89)	2.78 (2.22–5.43)	2.66 (2.65–2.68)	2.65 (2.50–2.91)
MgO	0.06 (0.00–0.19)	0.21 (0.00–1.11)	0.01 (0.00–0.02)	0.21 (0.05–0.46)
FeO	0.43 (0.34–0.59)	0.42 (0.23–1.04)	0.42 (0.33–0.56)	0.41 (0.36–0.45)
MnO	0.04 (0.00–0.09)	0.03 (0.00–0.07)	0.02 (0.00–0.05)	0.03 (0.01–0.07)
Al_2O_3	20.85 (19.50–21.32)	21.08 (20.37–22.94)	21.11 (21.02–21.17)	20.24 (19.52–20.93)
Cr_2O_3	0.01 (0.00–0.02)	0.01 (0.00–0.03)	0.00 (0.00–0.01)	0.00 (0.00–0.01)
SiO_2	62.63 (61.41–63.52)	62.35 (58.52–63.38)	63.14 (63.09–63.17)	63.97 (63.35–65.16)
TiO_2	0.01 (0.00–0.04)	0.01 (0.00–0.04)	0.01 (0.00–0.02)	0.00 (0.00–0.01)
Total	97.97 (96.27–98.99)	98.17 (96.45–99.47)	98.93 (98.74–99.10)	98.59 (97.85–98.97)
Ab	86.76 (85.28–88.94)	85.68 (75.24–88.14)	86.00 (85.64–86.23)	85.49 (84.45–87.25)
An	11.22 (9.66–12.65)	12.14 (9.68–23.93)	11.41 (11.32–11.54)	11.88 (10.68–12.58)
Or	2.02 (1.39–2.90)	2.18 (0.82–2.95)	2.59 (2.45–2.82)	2.63 (2.07–2.97)

Table 5. Microprobe data for iron (Irn), taenite (Tae), and tetrataenite (Tet) (wt.%).

	Irn	Irn	Irn	Tae	Tet	Tet
	Type 4	Type 5	Vein	Type 4	Type 5	Vein
N	**8**	**6**	**9**	**1**	**1**	**1**
Fe	93.02 (92.45–93.66)	93.43 (92.54–93.87)	93.72 (92.88–94.79)	62.16	47.19	47.20
Ni	6.44 (6.14–6.76)	6.34 (6.01–6.64)	6.15 (5.72–6.57)	37.11	52.93	52.62
Co	0.41 (0.39–0.43)	0.40 (0.35–0.42)	0.41 (0.37–0.44)	0.13	0.07	0.15
P	0.00 (0.00–0.01)	0.00 (0.00–0.01)	0.00 (0.00–0.01)	0.02	0.00	0.00
Al	0.01 (0.00–0.02)	0.00 (0.00–0.00)	0.00 (0.00–0.02)	0.00	0.00	0.00
Cr	0.01 (0.00–0.02)	0.00 (0.00–0.01)	0.01 (0.00–0.03)	0.00	0.00	0.01
S	0.01 (0.00–0.01)	0.00 (0.00–0.01)	0.01 (0.00–0.02)	0.02	0.00	0.05
Ti	0.01 (0.00–0.02)	0.00 (0.00–0.01)	0.01 (0.00–0.02)	0.00	0.01	0.00
Si	0.00 (0.00–0.01)	0.00 (0.00–0.01)	0.01 (0.00–0.02)	0.00	0.00	0.00
Total	99.91 (99.03–100.68)	100.17 (99.57– 100.52)	100.32 (99.52– 101.51)	99.44	100.20	100.03
Formula	$Fe_{0.93}Ni_{0.06}$	$Fe_{0.94}Ni_{0.06}$	$Fe_{0.94}Ni_{0.06}$	$Fe_{0.64}Ni_{0.36}$	$Fe_{0.97}Ni_{1.03}$	$Fe_{0.97}Ni_{1.03}$

Table 6. Microprobe data for troilite (wt.%).

	Type 4	Type 5	Vein
N	**5**	**6**	**5**
Fe	61.46 (60.73–61.99)	62.06 (61.83–62.54)	61.85 (60.93–62.57)
Ni	0.05 (0.00–0.14)	0.03 (0.00–0.08)	0.01 (0.00–0.02)
Co	0.01 (0.00–0.02)	0.01 (0.00–0.03)	0.00 (0.00–0.00)
S	35.49 (34.60–36.35)	36.00 (35.53–36.92)	35.68 (34.88–36.43)
P	0.00 (0.00–0.01)	0.00 (0.00–0.00)	0.00 (0.00–0.02)
Al	0.03 (0.00–0.09)	0.01 (0.00–0.03)	0.03 (0.00–0.09)
Cr	0.01 (0.00–0.03)	0.01 (0.00–0.03)	0.01 (0.00–0.04)
Ti	0.00 (0.00–0.01)	0.00 (0.00–0.01)	0.00 (0.00–0.01)
Si	0.00 (0.00–0.01)	0.00 (0.00–0.01)	0.00 (0.00–0.01)
Total	97.05 (96.12–98.25)	98.12 (96.98–99.42)	97.58 (96.11–98.61)
Formula	$Fe_{1.00}S_{1.00}$	$Fe_{0.99}S_{1.00}$	$Fe_{1.00}S_{1.00}$

Neumann lines in iron, in addition to the presence of shock melt veins and melt pockets indicate a shock stage S3/S4 of Stöffler *et al.* (1991).

The mol percent fayalite *vs.* the mol percent ferrosilite plots within the H group, according to Figure 8.

The cobalt content in iron (average composition in weight percent) *vs.* fayalite in olivine (mol percent) in the chondrules also lies within the H group range (Fig. 9).

Using the pyroxene analyses, we calculated the percent mean deviation (PMD) of ferrosilite in enstatite for each clast and they present no visible difference seeming to represent H4 low and high borders. PMD of 5.44, 9.16 and 18.13 (at vein), respectively, corresponding to petrologic type 4 chondrites.

Olivine, low-Ca, and high-Ca pyroxene chemical compositions were analyzed in each of the major clasts and in the melt vein. The mol% compositions of ferrosilite and fayalite plot within the H group. Its petrologic type matches those of other clasts with the matrix as petrologic type 4.

As a typical result for a thermal metamorphic chondrite, such as petrologic type 4 to 6, the striking feature of cathodoluminescence of Parauapebas meteorite is the blue color dominance in the mesostasis of chondrules opposing the lack of luminescence into the olivine and pyroxenes grains (Fig. 10).

DeHart *et al.* (1992) and Sears *et al.* (1992) developed the compositional classification scheme for chondrules, taking into

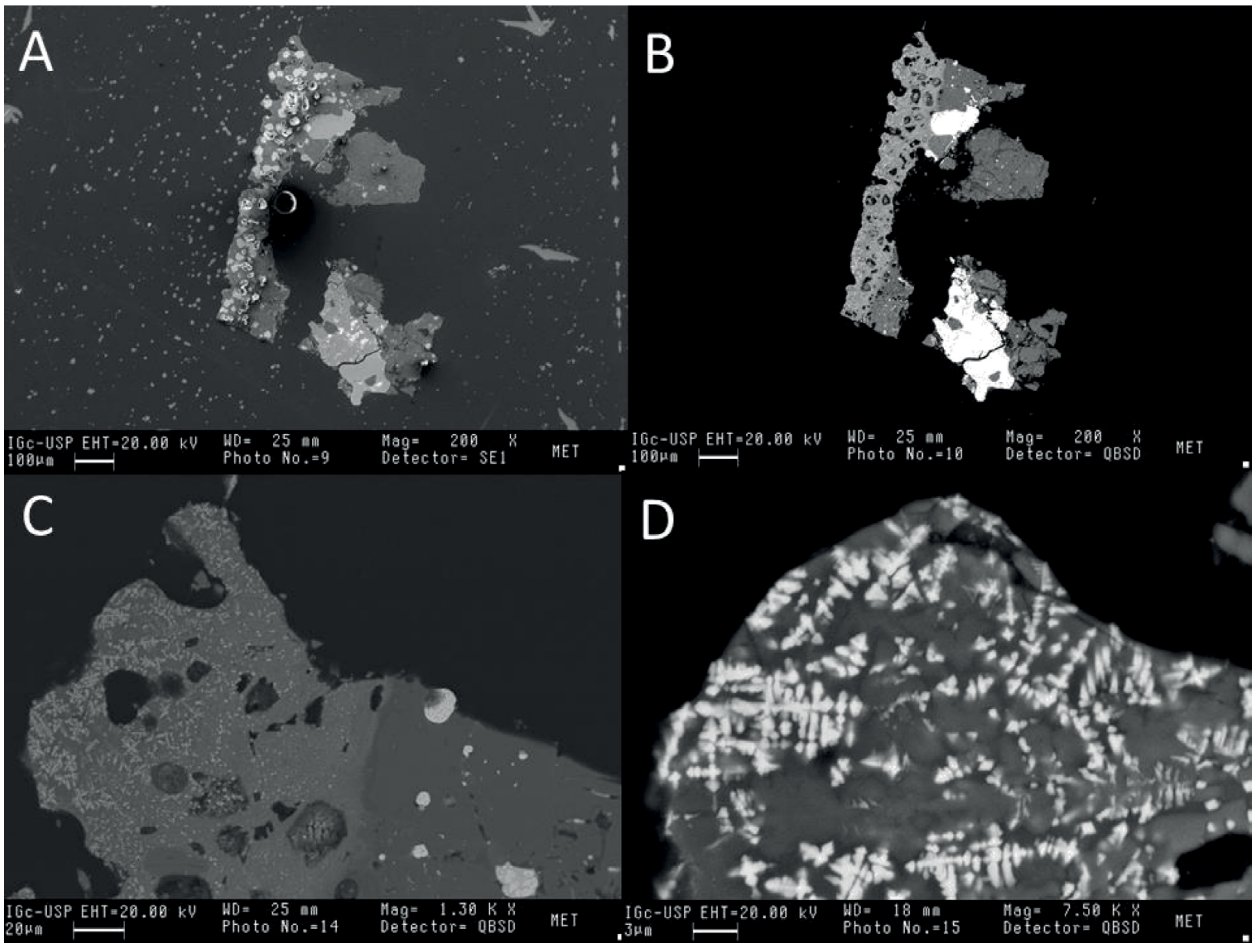

Figure 7. (A) Secondary electrons and (B) backscattered electrons images of the fusion crust (left grain, lighter gray in the second image), showing vesicles and iron oxide dendrites. (C) Detail of the fusion crust. (D) Iron oxide dendrites in the fusion crust.

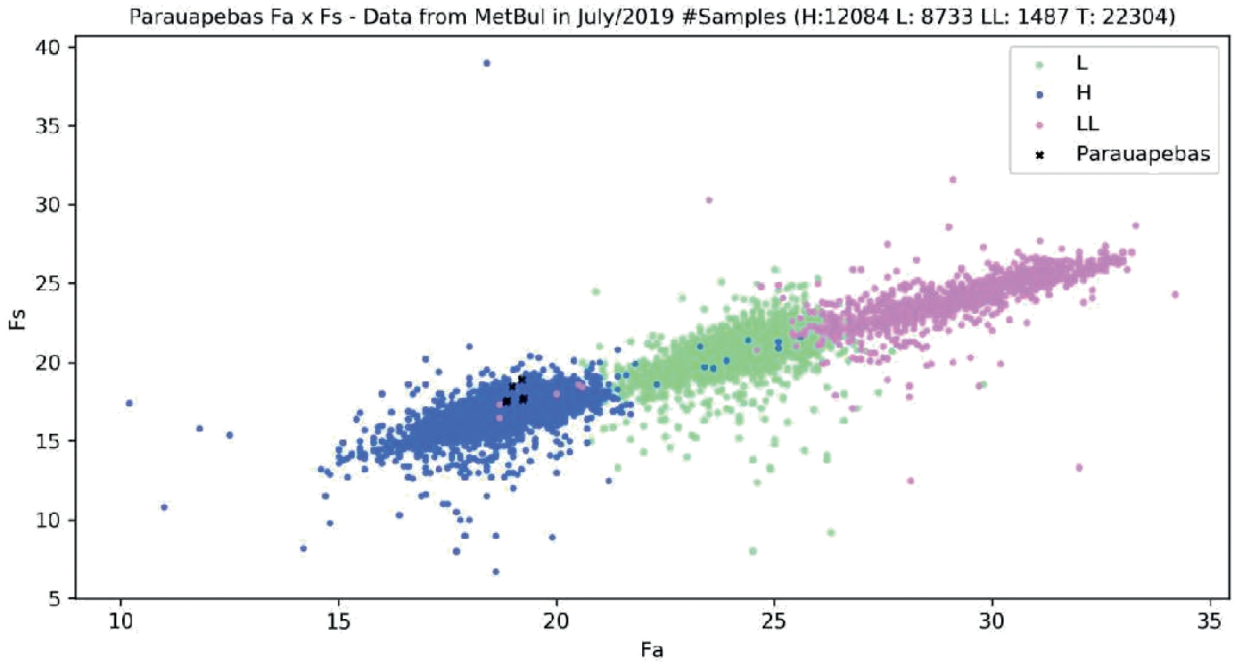

Figure 8. Fayalite (mol %) versus ferrosilite (mol %) distribution of ordinary chondrites showing the H, L, and LL groups.

account the CL colors emitted by minerals. In terms of CL, there are two main trends, one that starts with luminescent chondrules and one that starts with non-luminescent ones. Thus, group A was designated to the brightest chondrules while group B gathered chondrules with low or no luminescence.

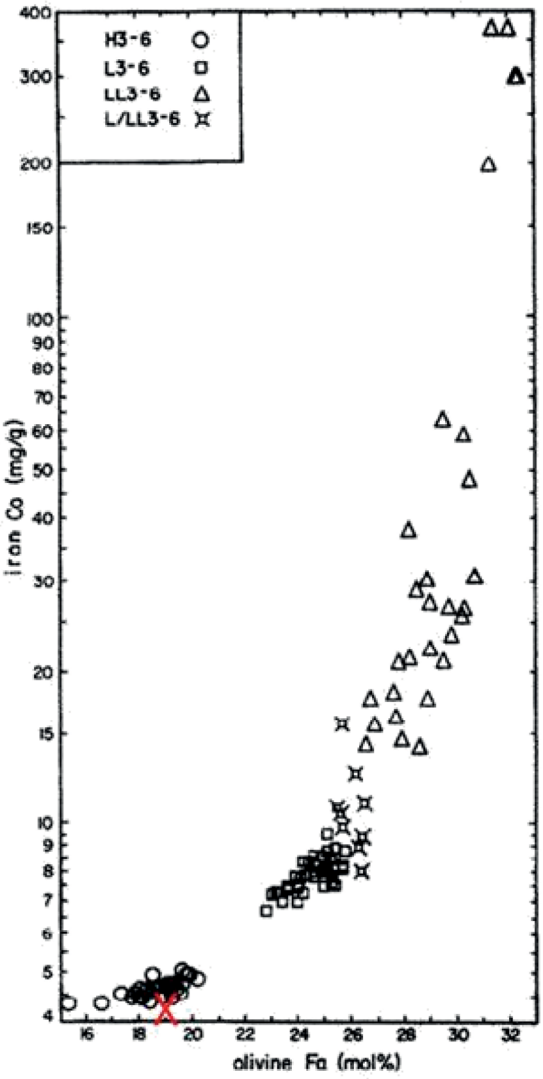

Figure 9. Co (wt %) in niron throughout the sample *versus* fayalite (mol %) in olivine.

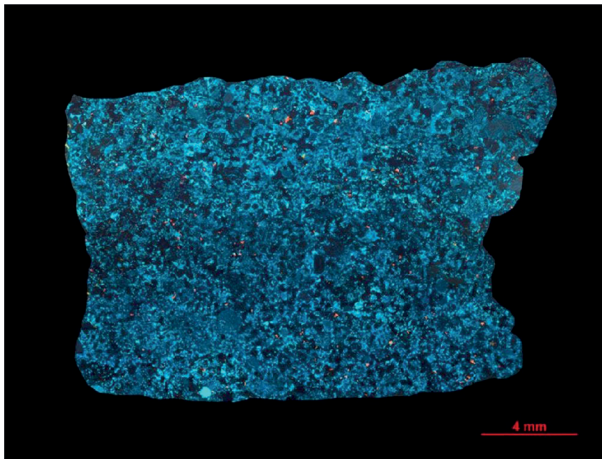

Figure 10. Cathodoluminescence image of Parauapebas meteorite.

DeHart (1989) correlated the petrologic types of chondrites 1 to 6 from those developed by Van Schmus and Wood (1967) and subtypes into the most primitive meteorites type 3 (3.0 to 3.9), as suggested by Sears *et al.* (1980) with CL color as well as with the mineral composition. These petrologic subtypes were created to split the type 3 meteorites, which exhibited slight mineral chemical and texture differences due to subtle thermal metamorphism events, where type 3.0 is designated to represent the most pristine materials, whereas types 3.1 to 6 indicate an increasing degree of petrologic equilibration and recrystallization (Weisberg *et al.* 2006). Thereby, the chondrules belonging to type A show highly blue plagioclase mesostasis (except the yellow Ca-rich mesostasis from the lowest petrologic subtypes, such as 3.0 to 3.2) and red olivine and pyroxene associated with Fe-poor minerals, whereas type B presents quartz mesostasis and Fe-rich olivine and pyroxenes.

According to Sears *et al.* (2013), as metamorphism proceeds, the chondrules undergo systematic changes until the two trends evolve into the uniform blue CL characteristic of equilibrated chondrules (Fig. 11). As shown in the figure, the three types present in chemically unequilibrated chondrules are A1, B1, and an unequilibrated type A5 (A5un) with reddish edges. Under the progress of metamorphism, these converge to the equilibrated type A5, passing through this process by intermediary groups A2, A3, A4, B2, and B3. For instance, the unequilibrated ordinary chondrites (UOC) as Sermakona (3.0) and Bishuspur (3.1) show colorful and brilliant CL results inside the chondrules with a dark glass matrix and the most metamorphosed ones have the blue recrystallized matrix and mesostasis with no luminescence olivine and pyroxenes, such as the Parauapebas meteorite. This behavior is explained by the fact that in the most primitive meteorites, mesostasis and olivine have a varied composition, whereas in meteorites of greater petrologic type, the composition is more homogeneous (Sears *et al.* 1992). The smallest yellow and red CL grains in the bulk are apatite that exhibit a great CL signal as their luminescence properties.

Therefore, based on this CL compositional classification, Parauapebas is clearly a high-petrologic type meteorite due to the absence of CL class A1, A2, A3, B1, B2, and B3 with the dominance of A5 (Fig. 12), the almost entirely CL signal of Parauapebas is related to type A5, even the melted vein, which splits both the petrological types of the meteorite, classified mainly by the subtle petrological differences in the matrix and in visible chondrites. This convergence to A5 equilibrated state occurs because the heat (> 300°C) turns Fe-poor in Fe-rich olivine and pyroxene with no CL and the glass around begins to recrystallize to plagioclase phases showing blue luminescence, as can be seen in the most part of this mass with dominance of the blue CL signal. Fayalite becomes chemically homogeneous from UOC 3.4 and ferrosilite from UOC 3.8 up to 4, whereas the matrix and mesostasis glasses recrystallize from the petrologic type 3.2 (Huss *et al.* 2006).

It confirms the highest petrologic classifications as type 5 for the biggest part of the Parauapebas meteorite, due to a sequence of soft chemical modifications along the thermal events submitted to the large mass of its parent body.

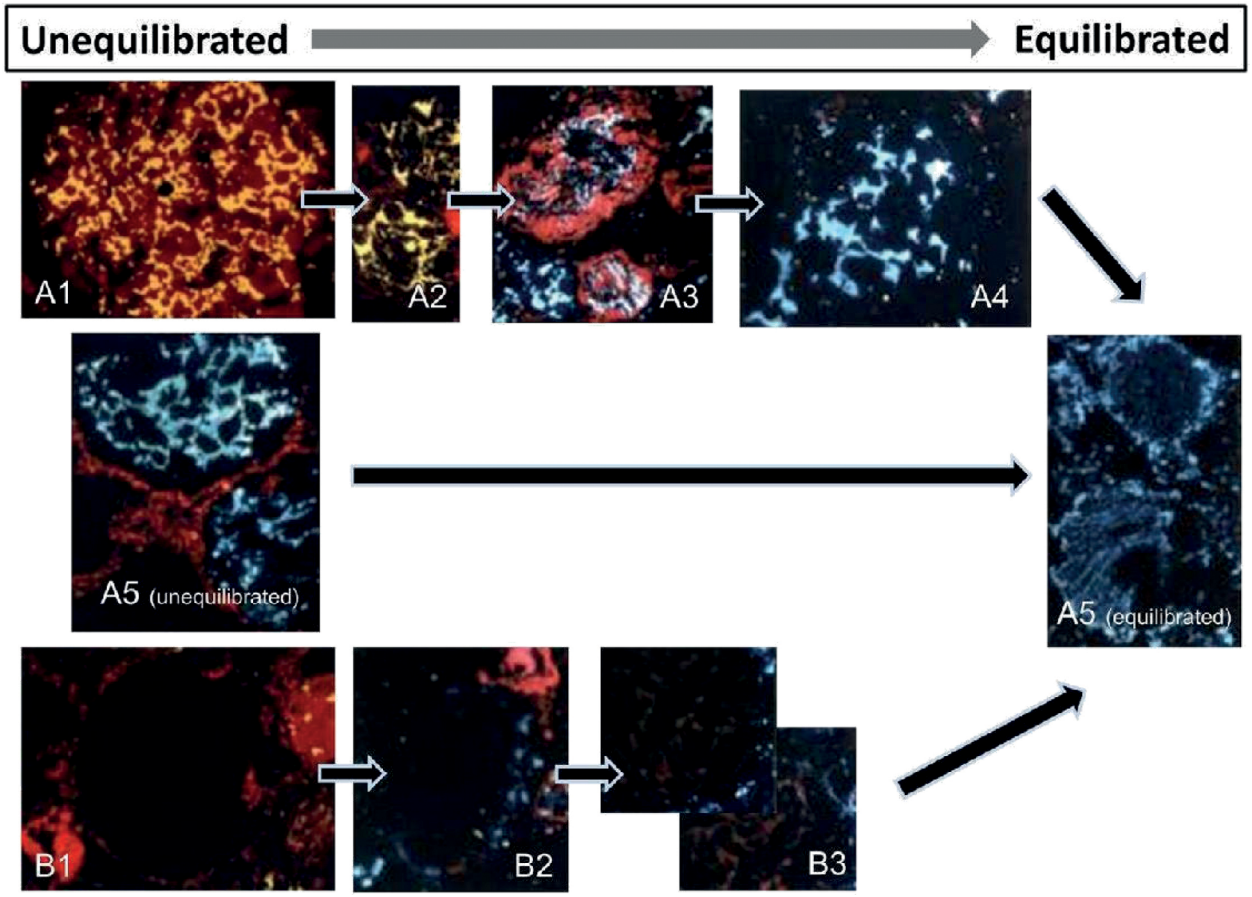

Figure 11. Schematic sequence of chemical equilibration of the chondrules. The cathodoluminescence images of chondrules showing the variations that occur during the thermal metamorphism in chondrites. The group A was designated to the brightest chondrules while group B gathered chondrules with low or no luminescence. Sears *et al.* (2013).

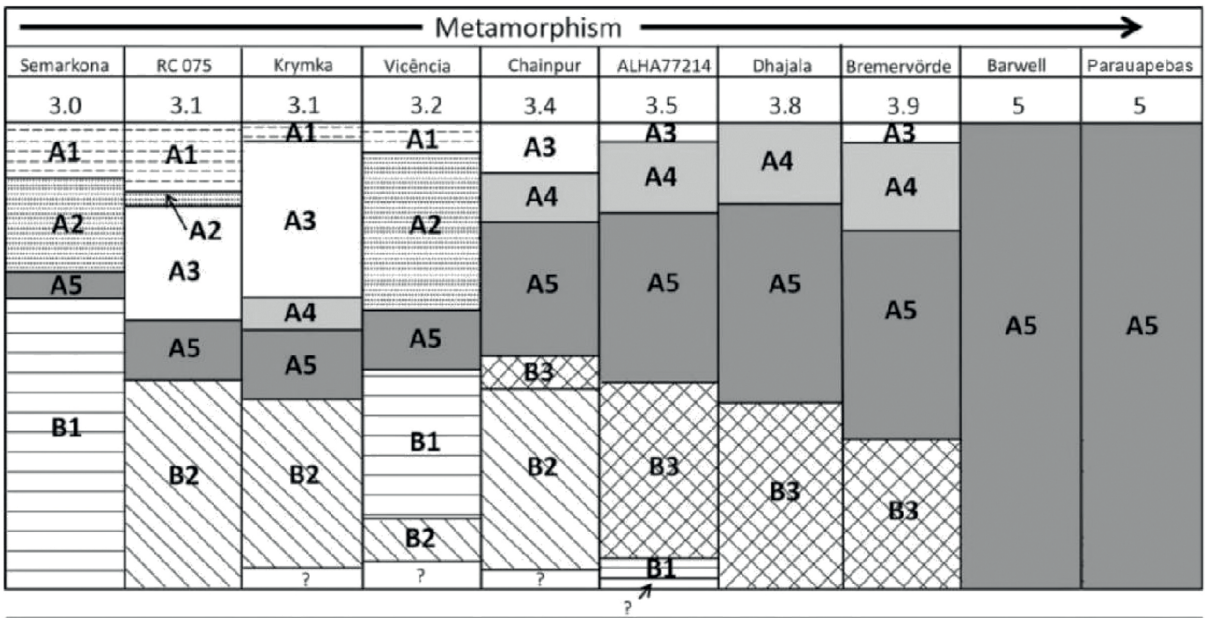

Figure 12. Distribution of chondrules in % of their total numbers across the chemical classes (defined by DeHart *et al.* 1992, Sears *et al.* 1992) in different petrologic types of chondrites from 3.0 to 5. Parauapebas is dominated by equilibrated chemical class A5 and classified as a high petrologic type 5. Clearly, Parauapebas is a high petrologic type meteorite due to the absence of CL class A1, A2, A3, B1, B2, and B3 with the dominance of A5. Scheme adapted from Keil *et al.* (2015).

ARTICLE INFORMATION
Manuscript ID: 20190085. Received on: 09/01/2019. Approved on: 05/24/2020.
D.A.: chemical and textural analysis by SEM/EDS, mineralogical identification, formula calculations, interpretation of results, text writing, general coordination of the works. D.C.: Obtained the first sample, historical data of meteorite's fall and recovery, chemical and textural analysis by SEM/EDS. A.M.: Obtained the second sample, historical data of the meteorite's fall and recovery, minerals calculations and statistical treatment of the microprobe analysis, making of graphs, submission to the Meteorite Bulletin Committee and registering the USP Institute of Geoscience as an official meteorite repository. M.Z.: Study of petrographic slides and polished sections, microprobe analysis, cathodoluminescence studies, interpretation of results, text writing. A.T.: Study of petrographic slides and polished sections, microprobe analysis, cathodoluminescence studies, interpretation of results, text writing. C.V.: Microscopic studies.
Competing interests: The authors declare no competing interests.

REFERENCES

Buchwald V.F.B. 1975. *Handbook of iron meteorites*. Berkeley: University of California Press. 3 v.

Burke E.A.J. 2006. A mass discreditation of GQN minerals. *Canadian Mineralogist*, **44**(6):1557-1560. http://dx.doi.org/10.2113/gscanmin.44.6.1557

DeHart J.M. 1989. *Cathodoluminescence and Microprobe Studies of the Unequilibrated Ordinary Chondrites*. PhD Thesis, University of Arkansas, Fayetteville.

DeHart J.M., Lofgren G.E., Jie L., Benoit P.H., Sears D.W.G. 1992. Chemical and physical studies of chondrites: X. Cathodoluminescence and phase composition studies of metamorphism and nebular processes in chondrules of type 3 ordinary chondrites. *Geochimica et Cosmochimica Acta*, **56**(10):3791-3807. https://doi.org/10.1016/0016-7037(92)90171-E

Dreher A.M., Dall'agnol R., Martini S.L. 1995. The Ipitinga H5 chondrite: a new meteorite found in Pará state, Northern, Brazil. *Anais da Academia Brasileira de Ciências*, **67**(1):45-54.

Gooding J.L., Keil K. 1981. Relative abundances of chondrule primary textural types in ordinary chondrites and their bearing on conditions of chondrule formation. *Meteoritics*, **16**(1):17-43. https://doi.org/10.1111/j.1945-5100.1981.tb00183.x

Hezel D.C., Poole G.M., Hoyes J., Coles B.J., Unsworth C., Albrecht N., Smith C., Rehkämper M., Pack A., Genge M., Russell S.S. 2015. Fe and O isotope composition of meteorite fusion crusts: Possible natural analogues to chondrule formation? *Meteoritics & Planetary Science*, **50**(2):229-242.

Keil K., Zucolotto M.E., Krot A.N., Doyle P.M., Telus M., Krot T.V., Greenwood R.C., Franchi I.A., Wasson J.T., Welten K.C., Caffee M.W., Sears D.W.G., Riebe M., Wieler R., dos Santos E., Scorzelli R.B., Gattacceca J., Lagroix F., Laubenstein M., Mendes J.C., Schmitt-Kopplin P., Harir M., Moutinho A.L.R. 2015. The Vicência meteorite fall: A new unshocked (S1) weakly metamorphosed (3.2) LL chondrite. *Meteorit Planet Sci*, **50**:1089-1111. doi:10.1111/maps.12456

Huss G.R., Rubin A.E., Grossman J.N. 2006. Thermal metamorphism in chondrites. *In*: Lauretta D.S.; McSween Jr. H.Y. (Eds.). *Meteorites and the Early Solar System II*. Tucson: University of Arizona Press, p. 567-586.

Ramdohr P. 1967. Die Schmelzkruste der Meteoriten. *Earth and Planetary Science Letters*, **2**(3):197-209. https://doi.org/10.1016/0012-821X(67)90129-X

Sears D.W.G., Grossman J.N., Melcher C.L., Ross L.M., Mills A.A. 1980. Measuring the metamorphic history of unequilibrated ordinary chondrites. *Nature*, **287**:791-795. https://doi.org/10.1038/287791a0

Sears D.W.G., Jie L., Benoit P.H., DeHart J.M., Lofgren G.E. 1992. A compositional classification scheme for meteoritic chondrules. *Nature*, **357**:207-210. https://doi.org/10.1038/357207a0

Sears D.W.G., Ninagawa K., Singhvi A.K. 2013. Luminescence studies of extraterrestrial materials: Insights into their recent radiation and thermal histories and into their metamorphic history. *Geochemistry*, **73**(1):1-37. https://doi.org/10.1016/j.chemer.2012.12.001

Stöffler D., Keil K., Scott E.R.D. 1991. Shock metamorphism of ordinary chondrites. *Geochimica Cosmochimica Acta*, **55**:3845-3867.

Swindel Jr. G.W., Jones W.B. 1954. The Sylacauga, Talladega County, Alabama, Aerolite. *Meteoritics*, **1**(2):125-132. https://doi.org/10.1111/j.1945-5100.1954.tb01323.x

Van Schmus W.R., Wood J.A. 1967. A chemical-petrologic classification for the chondritic meteorites. *Geochimica Cosmochima Acta*, **31**(5):747-765. https://doi.org/10.1016/S0016-7037(67)80030-9

Weisberg M.K., McCoy T.J., Krot A.N. 2006. Systematics and evaluation of meteorite classification. *In*: Lauretta D.S., Mc Sween Jr. H.Y. (Eds.). *Meteorites and the Early Solar System II*. Tucson: University of Arizona Press, p. 19-52.

Yin Q.Z., Zhou Q., Sanborn M.E., Ziegler K., Li Q.L., Liu Y., Li C.L. 2019. Petrography and U-Pb chronology of anomalous eucrite Serra Pelada. In: Annual Meeting of The Meteoritical Society, 82., 2019. *Annals...*

Zucolotto M.E., Tosi A.A., Villaça C.V.N., Moutinho A.L.R., Andrade D.P.P., Faulstich F., Gomes A.M.S., Rios D.C., Rocha M.C. 2018. Serra Pelada: the first Amazonian Meteorite fall is a Eucrite (basalt) from Asteroid 4-Vesta. *Anais da Academia Brasileira de Ciências*, **90**(1):3-16. http://dx.doi.org/10.1590/0001-3765201820170854